SoftwareX 34 (2026) 102669

Contents lists available at ScienceDirect

SoftwareX

journal homepage: www.elsevier.com/locate/softx

HIT: A fully automated mosaicking software for corneal confocal microscopy

Stephan Allgeier[a,1,*], Klaus-Martin Reichert[a,1], Ekaterina Korn[a], Ralf Mikut[a], Sebastian Bohn[b,c], Oliver Stachs[b,c], Karsten Sperlich[b,c]

[a] Institute for Automation and Applied Informatics, Karlsruhe Institute of Technology (KIT), Karlsruhe, Germany
[b] Department of Ophthalmology, Rostock University Medical Center, Rostock, Germany
[c] Department Life, Light & Matter, University of Rostock, Rostock, Germany

ARTICLE INFO

Keywords:
Image mosaicking
Image registration
In vivo imaging
Corneal confocal microscopy

ABSTRACT

In vivo confocal microscopy (IVCM) provides high-quality image data of the living human cornea with cellular resolution. Leveraging the diagnostic potential of IVCM of the subbasal nerve plexus and corneal immune cells, in particular, is an active field of research. However, the small field of view of high-resolution IVCM represents a serious limitation for many possible applications. The presented software *HIT* creates motion-corrected wide-field montages from large IVCM image datasets and overcomes the shortcomings of other approaches. *HIT* is a cross-platform, open-source C++ software and provides its fully automated workflow with a straightforward graphical user interface. *HIT* makes state-of-the-art mosaicking software for large IVCM datasets widely available and opens up entirely new opportunities for all research groups in this field.

Metadata

Code metadata.

Nr.	Code metadata description	Metadata
C1	Current code version	v1.2.0
C2	Permanent link to code/repository used for this code version	https://github.com/KIT-IAI/HRT-Imaging-Tool
C3	Permanent link to Reproducible Capsule	None
C4	Legal Code License	GNU General Public License version 2 (GPL-2.0)
C5	Code versioning system used	git
C6	Software code languages, tools, and services used	C++
C7	Compilation requirements, operating environments & dependencies	CMake environment, cross-platform (tested under Microsoft Windows 11 with Microsoft Visual Studio 2022 and under Ubuntu Linux 22.04 with Visual Studio Code and CMake 4.2.1)
C8	If available Link to developer documentation/manual	https://gitlab.kit.edu/kit/iai/ml4time/cornea/hit
C9	Support email for questions	stephan.allgeier@kit.edu

* Corresponding author.
Email addresses: stephan.allgeier@kit.edu (S. Allgeier), klaus.reichert@kit.edu (K.-M. Reichert), ekaterina.korn03@gmail.com (E. Korn), ralf.mikut@kit.edu (R. Mikut), sebastian.bohn@uni-rostock.de (S. Bohn), oliver.stachs@uni-rostock.de (O. Stachs), karsten.sperlich@uni-rostock.de (K. Sperlich).
[1] Shared first authors.

https://doi.org/10.1016/j.softx.2026.102669
Received 17 February 2026; Received in revised form 8 April 2026; Accepted 17 April 2026
Available online 25 April 2026

Software metadata.

Nr.	(Executable) software metadata description	Please fill in this column
S1	Current software version	v1.2.0
S2	Permanent link to executables of this version	https://github.com/KIT-IAI/HRT-Imaging-Tool/releases/tag/v1.2.0
S3	Permanent link to Reproducible Capsule	None
S4	Legal Software License	GNU General Public License version 2 (GPL-2.0)
S5	Computing platforms/Operating Systems	Microsoft Windows / Ubuntu Linux
S6	Installation requirements & dependencies	None
S7	If available, link to user manual - if formally published include a reference to the publication in the reference list	https://gitlab.kit.edu/kit/iai/ml4time/cornea/hit
S8	Support email for questions	stephan.allgeier@kit.edu

1. Motivation and significance

The human cornea is integral for our visual system, contributing the largest amount of refraction along the path of incident light before it is detected on the retina. Imaging techniques play an important diagnostic role in assessing the physiological integrity of the corneal tissues. Thanks to its dense innervation with sensory nerve fibers and its transparent nature, the cornea also acts as a window to the peripheral nervous system. In particular, in vivo confocal microscopy (IVCM) has been established as the best available imaging technique to visualize the corneal subbasal nerve plexus (SNP). IVCM is used to detect pathological alterations of the SNP in a wide variety of diseases, such as diabetic neuropathy [1], multiple sclerosis [2], Parkinson's disease [3], long COVID [4], chemotherapy-induced neuropathy [5], or ocular diseases [6]. Moreover, immune cells (ICs) in the vicinity of the SNP can reflect corneal infections and inflammatory conditions [6] or an immune response to medication [7].

IVCM provides high-quality image data of the SNP nerve structures and corneal ICs at cellular resolution, particularly with laser-scanning devices. However, the high resolution of these systems is achieved at the expense of a relatively small field of view (FOV). For example, the widely used Heidelberg Engineering HRT-RCM typically images a FOV of $400\,\mu m \times 400\,\mu m$. For many diagnostic tasks, the small FOV is a significant limitation if the recorded image does not include the structure of interest in its entirety. Moreover, the SNP is known to exhibit strong local morphological variability [8–10]; morphological SNP parameters extracted from a single IVCM image therefore cannot support robust diagnostic conclusions. This can be mitigated by creating montage visualizations of an extended region of the SNP from multiple images. Unfortunately, standard-purpose image stitching tools are not appropriate for this use case, because corneal IVCM images are always to some degree affected by unavoidable motion artifacts, which manifest as characteristic, non-linear geometric distortions of the imaged tissue. They are due in part to fixational eye movements [11–13], but also because movement during the imaging process is inherently required to cover an extended corneal area.

Several dedicated algorithmic mosaicking techniques have been published [14–20]. Some of them rely on specific (hardware) setups for the imaging process, restricting their wider usability, and the vast majority of the software solutions for IVCM image registration and wide-field image montage are not publicly available. The only two current exceptions are the Python-based algorithms *NerveStitcher* [21] and *NerveStitcher2.0* [22]; both are free and open-source software (OSS). *NerveStitcher* implements neural networks to extract feature points and associated point descriptors from single IVCM images, and to match feature points between images. From the point correspondences between an image pair, *NerveStitcher* derives a translation vector that is used to align the two images (and iteratively the remaining images of an IVCM image sequence) and create a wide-field montage. *NerveStitcher2.0* improves the *NerveStitcher* algorithm with an optical flow module that evaluates the image pair registrations and excludes erroneous alignment results. Both *NerveStitcher* tools are script-based and require the input data to be specified in the source code. Both also share two common algorithmic shortcomings. First, they only successively add additional images to a growing mosaic image; after adding an image, its alignment information cannot be adjusted later. This raises the problem of accumulating registration errors along paths with recurring positions, for example a simple circular loop. If small registration errors accumulate over the image pair registrations along the path, the image that closes the circle cannot be placed appropriately to align with the preceding image and the first image of the sequence at the same time. This is a known problem in real-world mosaicking applications [23]. The second significant shortcoming is their limitation to translational transformations when aligning the IVCM images. They are therefore incapable of handling the inherent IVCM motion artifacts appropriately.

The present contribution describes *HIT* (which stands for *HRT Imaging Tool*), an OSS solution for the task described above. *HIT* is not a general-purpose image registration framework, but is deliberately tailored to process large datasets of HRT-RCM image data. Despite its complex algorithmic interior, the automated workflow is controlled by very few parameters, and many use cases are covered by the default preset parameters. The parameter adjustment and the actual process pipeline are accessible via straightforward graphical user interfaces (GUIs). In the overall clinical workflow, *HIT* is intended for offline processing of previously acquired image datasets. This can either take place immediately after the examination, for fast assessment of the image data in the presence of the patient, or it may occur much later, for instance to batch process multiple datasets in a clinical study setting.

Diverse purposes can benefit from SNP mosaic images, for example to

- provide a more reliable basis for quantitative morphology measures of the SNP [9,10,24],
- examine geometric relations between different corneal structures (e.g., ICs and subbasal nerves) [25,26],
- pinpoint the imaged region of the cornea (using anatomical features such as the inferior whorl) [25,27–32], or
- establish relative alignment between recurring examinations to investigate cell migration, disease progression, or therapy response, in the exact same corneal area [5,7,33,34].

2. Software description

A typical complete workflow for large-area IVCM of the SNP starts with the imaging procedure, followed by a preparatory dataset creation step, the mosaic image creation using *HIT*, and finally a specific analysis task (see Fig. 1).

HIT expects image data recorded with the HRT-RCM system, which can be sets of manually triggered images, automatically recorded continuous image sequences, or focus stacks. In the vast majority of use cases, the data to be processed into an extended mosaic image (or volume representation) will be from a single examination. In principle, the image data may also originate from several examination sessions, as long as the imaged tissue remains largely unchanged morphologically and geometrically, and the head position of the examined person is reproduced with sufficient accuracy to ensure that all image data has the same rotational alignment.

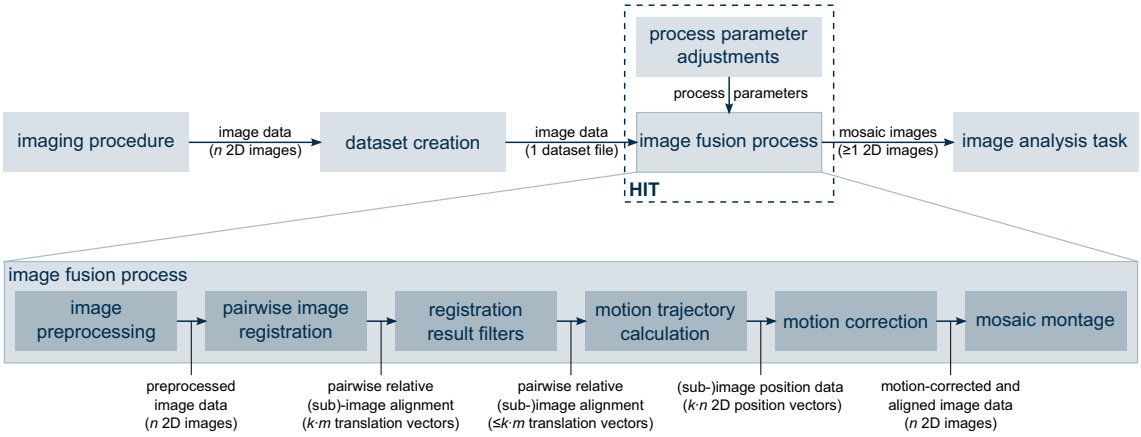

Fig. 1. Overview of a complete, typical IVCM workflow that involves *HIT*. The dashed box marks the steps implemented in the *HIT* software. The bottom row shows the internal algorithmic steps of the *HIT* image fusion process. (n: dataset size; m: number of successfully registered image pairs; k: number of sub-images per image).

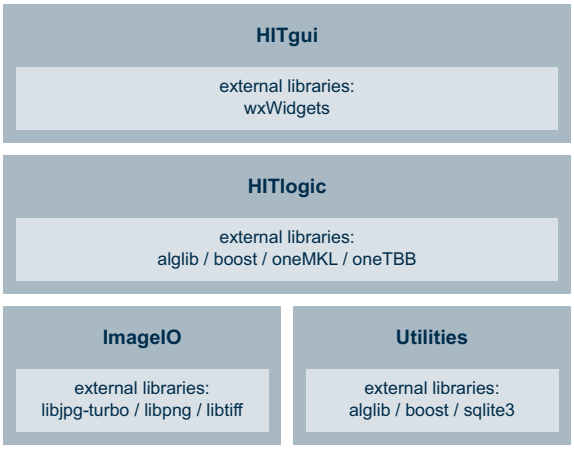

Fig. 2. Overview of the *HIT* software architecture.

The input data unit for the internal *HIT* pipeline is the *dataset*. A dataset contains all the image data to be montaged into a mosaic image. *HIT* requires a separate, multi-page TIFF dataset file for each dataset. Each page in the dataset file represents a single image frame (384 × 384 pixels, 8-bit pixel depth). Because the HRT software itself does not support export to multi-page TIFF files, users need to use an external tool in the dataset creation step, for example the free OSS *Fiji* [35]. The multi-page TIFF file is created from raw HRT image files, without any additional filtering or other preprocessing.

The GUI-based usage of *HIT* is straightforward. The user may first review and adjust the effective process parameters in the parameter dialog GUI (see Section 2.2.1). Process parameters are stored persistently and reused until they are explicitly changed. The main *HIT* GUI allows the user to specify an arbitrary number of datasets for sequential batch processing. The actual execution is fully automated. Section 2.2.2 provides additional details on the output structure of the results.

2.1. Software architecture

The software architecture of *HIT* is separated into four components, as visualized in Fig. 2. The component **ImageIO** collects image file import and export classes. The component **Utilities** contains a variety of basic-level support classes. The component **HITlogic** implements the image processing framework, including representations for datasets, pipeline steps, and result structures. The top-level component **HITgui** implements the GUI. All components use external, portable OSS libraries (see Fig. 2). All external libraries, except for *alglib*, are imported through the *vcpkg* package manager. The OSS-licensed *alglib* source files are included in the *HIT* project directly. The *alglib* library is also available in a commercial-license version, which brings some advantages, such as improved parallelization. To build *HIT* with that version of *alglib*, the source files are simply replaced by their commercial-license counterparts.

2.2. Software functionalities

The internal image processing pipeline of *HIT* can be broken down into several successive steps (see Fig. 1).

An optional **image preprocessing** step can perform preprocessing tasks on the image data, such as correcting the HRT-RCM-typical vignetting effect.

The **pairwise image registration** step is one of the core features of the *HIT* pipeline. Image pairs are selected from the dataset according to a predefined strategy [36,37]. The image pair registration operates on a sub-image level to enable motion artifact correction. The first image of a given pair is decomposed into rectangular, horizontal sub-images, which are then aligned to the second image using correlation-based image registration [38,39]. The correlation value (termed the score) of each correlation calculation is compared against a predefined score threshold; registration results with a below-threshold score are considered incorrect and are immediately discarded.

Optional **registration result filters** perform further in-depth analyses on the collected registration results to identify remaining incorrect results. The most important filter option is the automatic score threshold calculation, which provides a fully automated operation mode that removes the need for manual process parameter adjustments in many use cases.

The second core feature of the *HIT* pipeline is the **motion trajectory calculation**. It forms a large system of linear equations from the relative image pair registration results, with the global absolute sub-image positions as unknowns. Regularization terms are introduced to solve the equation system. If the image data represent a time-continuous image sequence, the resulting position coordinates are also time-continuous and describe the scene motion trajectory observed during the imaging process [39].

The **motion correction** step removes the motion-induced geometric distortions from the image data, based on the calculated sub-image positions [39] (see Fig. 3B). Optionally, the motion-corrected images can be exported to separate image files; in volume reconstruction workflows, these images form a focus stack.

Finally, a **mosaic montage** is created from the motion-corrected image data by weighted averaging [18,36] (see Fig. 3C). If tissue class data

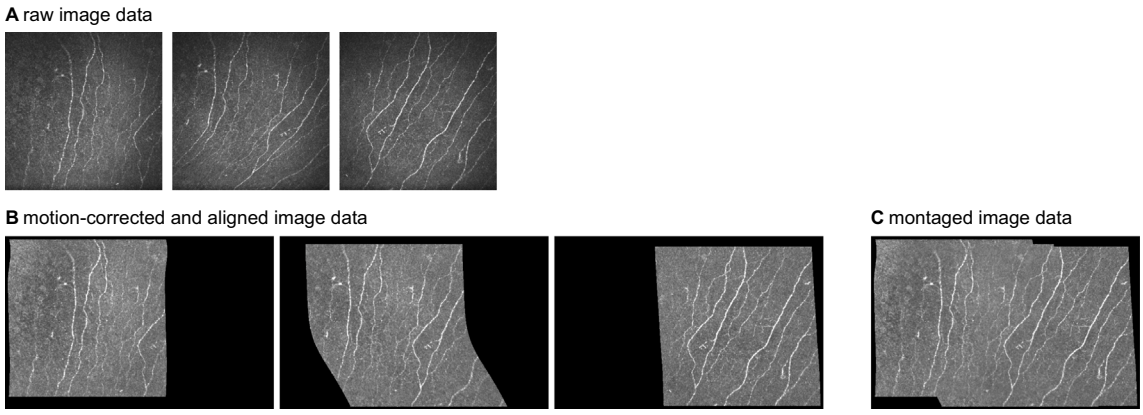

Fig. 3. Image data passing through the processing pipeline. (A) Example raw images (images 335, 336 and 337 of the dataset used in Section 3). (B) The example images after the motion correction step. (C) A montage of the motion-corrected example images.

```
data_root_folder
├─ dataset_id.tif
├─ dataset_id_results.tif
└─ dataset_id
   ├─ dataset_id_snp
   │  ├─ dataset_id_00000.tif
   │  ⋮
   │  └─ dataset_id_00099.tif
   └─ dataset_id_m
      ├─ dataset_id.sqlite
      ├─ dataset_id_m1.tif
      ├─ dataset_id_m2.tif
      ├─ dataset_id_m1
      │  ├─ dataset_id_00000_mc.tif
      │  ⋮
      │  ├─ dataset_id_00056_mc.tif
      │  ├─ dataset_id_00058_mc.tif
      │  ⋮
      │  └─ dataset_id_00099_mc.tif
      └─ dataset_id_m2
         └─ dataset_id_00057_mc.tif
```

Fig. 4. *HIT* data folder structure for an exemplary dataset, `dataset_id.tif`, which contains 100 images and yields two mosaic images: `dataset_id_m1.tif` (montage from all images except image 57) and `dataset_id_m2.tif` (identical to original image 57). The optional motion-corrected image files (filename suffix "`_mc`") are included.

```
-4.761;  8.265; -6.708; 1
-5.555;  7.973; -4.939; 1
-5.012;  8.733; -6.541; 1
-2.817; -2.217;  3.088; 2
-8.171; -2.714;  8.296; 2
-2.145; -3.068;  3.055; 2
-2.354;  3.291; -3.885; 1
-5.903; 10.318; -7.003; 1
-2.700;  4.419; -4.484; 1
 0.336; -0.501; -2.133; 0
 2.201; -3.101; -3.149; 0
 2.049; -3.504; -2.419; 0
 2.305; -2.927; -2.134; 0
 2.500; -2.604; -3.008; 0
 1.287; -1.639; -2.710; 0
-3.378;  6.934; -5.318; 1
-6.456; 10.958; -7.394; 1
```

Fig. 5. Excerpt from an exemplary tissue class file containing distance values from a multi-class support vector machine for the *Epithelium*, *SNP*, and *Stroma* tissue classes (blue), and the classification (green) of each image (For interpretation of the references to colour in this figure legend, the reader is referred to the web version of this article.).

are provided (see Section 2.2.3), non-SNP images may be excluded from the mosaic montage [18,40].

It is not always possible to establish the relative alignment for all images of a dataset, due to insufficient image overlap or unintentional focus changes. In this case, the images are divided into disjoint subsets, in which alignment has been established based on the pairwise image registration step. Each subset yields a separate mosaic image.

2.2.1. Process parameters

HIT provides a separate GUI to review and adjust all process parameters. It opens when the *HIT* executable is called with the "`-p`" command line flag. A list of the most relevant process parameters is provided in the Supplementary File.

2.2.2. File system structure

For each processed dataset, *HIT* creates a separate result folder structure within the directory where the dataset file resides (the data root folder). If a tissue class file is provided, it must reside in the data root folder and be named accordingly (see Fig. 4).

The result folder contains the created mosaic images and an SQLite database file that stores all relevant process metadata (i.e., the used process parameters), intermediate results (i.e., registration results and calculated position data), and mosaic image metadata (e.g., which images contribute to each mosaic image). Optionally exported motion-corrected single images reside in separate sub-folders for each mosaic image. Fig. 4 shows the complete data folder structure for an exemplary dataset.

Table 1
Mosaic image properties for example dataset.

Mosaic file	# included images	Mosaic area [mm^2]
`01_LE_m1.tif`	318	4.90
`01_LE_m2.tif`	1	0.16
`01_LE_m3.tif`	2	0.23
`01_LE_m4.tif`	83	2.02
`01_LE_m5.tif`	1	0.16
`01_LE_m6.tif`	1	0.16
`01_LE_m7.tif`	1	0.16

2.2.3. Tissue classification data

HIT can use supplementary tissue classification data for the mosaic montage step. These data must be provided in an appropriately named CSV file. The tissue class file format (see Fig. 5) requires exactly one line per image in the dataset, and four data entries per line, separated by semicolons.

The first three values per line may be any numerical entries, such as class-related likelihood values. The fourth value per line defines the actual class: 0 (*Epithelium*), 1 (*SNP*), 2 (*Stroma*), or -1 (*Undefined*). If the option to exclude non-SNP images is switched on, the mosaic montage is restricted to images with a class-entry of 1. This behavior can be used to create 2D mosaic images with other selection criteria (e.g., at other depth levels than the SNP), if all images to be montaged are specified by a class-entry of 1 (and all other images by other values).

3. Illustrative examples

We demonstrate the *HIT* workflow, using the dataset "`01_LE`" from the publicly available data repository of Badian et al. [41]. We use *Fiji* [35] to create a multi-page TIFF dataset file from the image data. To ensure that *HIT* uses appropriate process parameters, we open the parameter dialog GUI and apply the default parameter set (button "Defaults for 2D datasets", see Supplementary File). Finally, we open the main dialog GUI, add the dataset file, and start the mosaicking process.

For the example dataset with 407 images, the *HIT* registration workflow identifies 7 separate image groups. Table 1 lists the properties of the 7 resulting mosaic images and Fig. 6 displays the largest mosaic image, `01_LE_m1.tif`.

The example dataset takes 47 s to process on a common Windows PC (Intel Core i9-11900K CPU), with the following distribution on

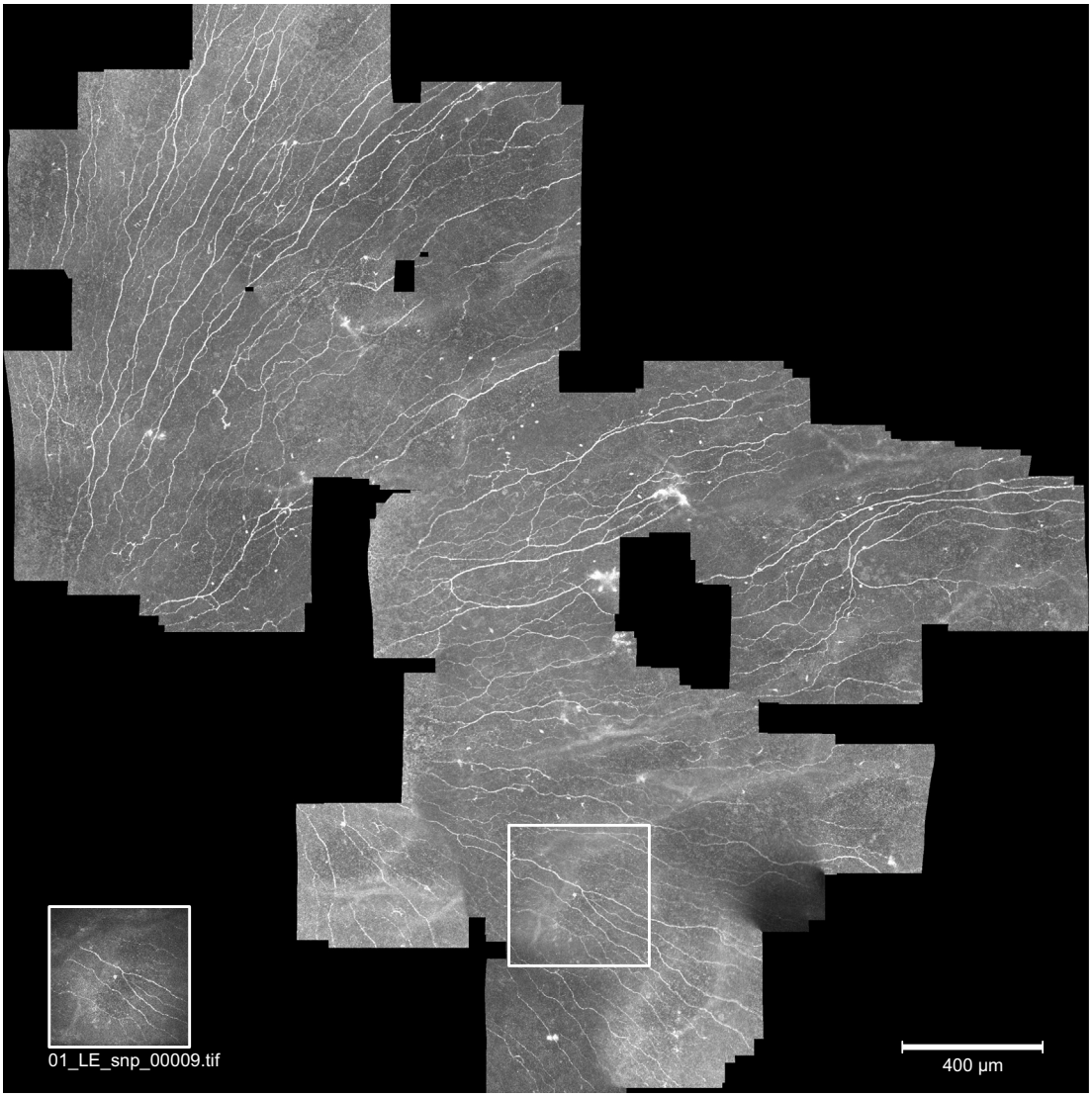

Fig. 6. Wide-field montage (`01_LE_m1.tif`) from the example dataset (original image data used from [41]). A single raw image from the dataset is presented in the bottom left corner; the white square frame shows its approximate position in the montage (For interpretation of the references to colour in this figure legend, the reader is referred to the web version of this article.).

processing steps: about 19 s for pairwise image registration, about 5 s for registration result filters, about 2 s for all other algorithmic steps together (image preprocessing, motion trajectory calculation, motion correction, and mosaic montage), and about 21 s for result file export (predominantly the SQLite database file).

4. Impact

Currently, the main application for *HIT* is to create large-area 2D montages of the corneal SNP from extended IVCM datasets. As such, it serves the same purpose as other software tools that have been proposed but are not widely available [14–17], as well as the two variants of *NerveStitcher* [21,22]. What sets *HIT* apart from other approaches and the key benefit for the target scientific community is its ability to correct motion artifacts, in addition to being OSS and easy to use. The application of *HIT* is not limited to SNP mosaics, however. It can also be used to create wide-field montages of corneal tissue at other focus depths [42].

First and foremost, automatically created large-area visualization of the SNP allows the assessment of SNP morphometry in large cohorts in various conditions or diseases. The extended FOV of the mosaic images effectively addresses the problem of local variability in morphological parameters [9,10]. If the image data contain detectable landmarks such as the inferior whorl pattern, these can be used to pinpoint the analyzed corneal region [25,27,28,32]. *HIT* has been used in several studies of SNP morphometry [3,27,43,44]. Other studies have used the *HIT* wide-field montages to study the presence, local distribution, or relative alignment of ICs in the vicinity of the nerves [25], the global distribution of subbasal nerve direction [29], or the larger arrangement of the inferior whorl [45]. Other recent examinations that relied on manually assembled wide-field montages [24,26,30,31] could benefit greatly from automated mosaicking.

In addition to the local variability of morphometric SNP parameters, the corneal subbasal nerves also exhibit characteristic global distribution patterns [45]. Longitudinal studies should therefore revisit the exact same corneal area in follow-up examinations, to remove potential parameter variability sources as much as possible. It has been shown that *HIT* mosaic images of the SNP taken weeks [34], months [5,7], or even more than a year apart [33] can be aligned with respect to each other, to precisely identify the overlapping corneal region. This is possible thanks to static structures, such as SNP nerve entry points, even though the migration of subbasal nerve fibers renders the SNP configuration as a whole unrecognizable after few weeks [34].

The possibility to align longitudinal mosaic images also opens the way to entirely new quantitative dynamic parameters, such as nerve migration rates [34] or IC motility. The first observations of IC motility were made within single aligned IVCM images [20,46], but this requires significant expertise from the IVCM operator and is limited to IC movements inside the FOV. These examinations could greatly benefit from large-area mosaicking [47].

Finally, the motion path of the examined eye, which is calculated (and exported) as an intermediate result in the mosaicking process of time-continuous image sequences, might be useful for entirely separate research questions.

For convenient reusability in external automated workflows, *HIT* provides an automation mode that is invoked using specific command line parameters (see Supplementary File for details) and uses widely available input and output file formats.

Even though *HIT* is specifically tailored for HRT-RCM image data, the implemented algorithmic techniques may have broader usability. In general, nothing prohibits adjustments to the registration pipeline to process image data from other confocal laser-scanning microscopy devices and specimens other than human eyes, as long as the FOV is scanned in a line-wise pattern and the image data consist of geometrically rigid scenes with translational but not rotational movements. With some adaptations, the general pipeline should also be applicable to other scanning microscopy imaging modalities, or even to specific use cases with image sequences of laterally moving scenes recorded with rolling-shutter cameras.

5. Conclusions

HIT is a cross-platform, C++, GUI-based application for the registration and fusion of HRT-RCM image sequences of the cornea, to boost research on large-scale morphological features of the SNP and corneal cell dynamics. It creates high-quality mosaics, often out-of-the-box with the default parameter presets.

HIT is being actively developed and improved; current work focuses on integrating a tissue classification module into *HIT*.

In conclusion, the present publication as OSS makes easy-to-use mosaicking software for large IVCM datasets widely available and opens up entirely new research opportunities for all research groups in this field.

CRediT authorship contribution statement

Stephan Allgeier: Writing – review & editing, Writing – original draft, Visualization, Validation, Supervision, Software, Project administration, Methodology, Investigation, Funding acquisition, Conceptualization. **Klaus-Martin Reichert:** Validation, Software, Methodology, Investigation, Conceptualization. **Ekaterina Korn:** Validation, Software, Methodology. **Ralf Mikut:** Writing – review & editing, Project administration, Conceptualization. **Sebastian Bohn:** Writing – review & editing, Validation, Conceptualization. **Oliver Stachs:** Writing – review & editing, Project administration, Conceptualization. **Karsten Sperlich:** Writing – review & editing, Validation, Project administration, Funding acquisition, Conceptualization.

Declaration of competing interest

The authors declare the following financial interests/personal relationships which may be considered as potential competing interests:

Stephan Allgeier reports financial support was provided by Deutsche Forschungsgemeinschaft. Karsten Sperlich reports financial support was provided by Deutsche Forschungsgemeinschaft. If there are other authors, they declare that they have no known competing financial interests or personal relationships that could have appeared to influence the work reported in this paper.

Acknowledgements

Parts of this work were funded by the Deutsche Forschungsgemeinschaft (DFG, German Research Foundation) – project number 469107515. We kindly acknowledge financial support from the KIT Publication Fund for the open access publication.

Appendix A. Supplementary data

Supplementary data to this article can be found online at doi:10.1016/j.softx.2026.102669.

References

[1] Roszkowska AM, Licitra C, Tumminello G, Postorino EI, Colonna MR, Aragona P. Corneal nerves in diabetes—the role of the in vivo corneal confocal microscopy of the subbasal nerve plexus in the assessment of peripheral small fiber neuropathy. Surv Ophthalmol 2021;66(3):493–513. https://doi.org/10.1016/j.survophthal.2020.09.003

[2] Bitirgen G, Akpinar Z, Malik RA, Ozkagnici A. Use of corneal confocal microscopy to detect corneal nerve loss and increased dendritic cells in patients with multiple sclerosis. JAMA Ophthalmol 2017;135(7):777. https://doi.org/10.1001/jamaophthalmol.2017.1590

[3] Andréasson M, Lagali N, Badian RA, Utheim TP, Scarpa F, Colonna A, Allgeier S, Bartschat A, Köhler B, Mikut R, Reichert K-M, Solders G, Samuelsson K, Zetterberg H, Blennow K, Svenningsson P. Parkinson's disease with restless legs syndrome—an in vivo corneal confocal microscopy study. npj Parkinsons Dis 2021;7:4. https://doi.org/10.1038/s41531-020-00148-5

[4] Bitirgen G, Korkmaz C, Zamani A, Ozkagnici A, Zengin N, Ponirakis G, Malik RA. Corneal confocal microscopy identifies corneal nerve fibre loss and increased dendritic cells in patients with long COVID. Br J Ophthalmol 2022;106(12):1635–41. https://doi.org/10.1136/bjophthalmol-2021-319450

[5] Stache N, Bohn S, Sperlich K, George C, Winter K, Schaub F, Do H-V, Röhlig M, Reichert K-M, Allgeier S, Stachs O, Stachs A, Sterenczak KA. Taxane-induced neuropathy and its ocular effects—a longitudinal follow-up study in breast cancer patients. Cancers 2023;15(9):2444. https://doi.org/10.3390/cancers15092444
[6] Ramirez-Miranda A, Guerrero-Becerril J, Ramirez M, Vera-Duarte G, Mangwani-Mordani S, Ortiz-Morales G, Navas A, Graue-Hernandez E, Alio J. In vivo confocal microscopy for corneal and ocular surface pathologies: a comprehensive review. Clin Ophthalmol 2025;19:1817–34. https://doi.org/10.2147/OPTH.S519705
[7] Sterenczak KA, Stache N, Bohn S, Allgeier S, Köhler B, Bartschat A, George C, Guthoff RF, Stachs O, Stachs A. Burst of corneal dendritic cells during trastuzumab and paclitaxel treatment. Diagnostics 2021;11(5):838. https://doi.org/10.3390/diagnostics11050838
[8] Vagenas D, Pritchard N, Edwards K, Shahidi AM, Sampson GP, Russell AW, Malik RA, Efron N. Optimal image sample size for corneal nerve morphometry. Optom Vis Sci 2012;89(5):812–7. https://doi.org/10.1097/OPX.0b013e31824ee8c9
[9] Winter K, Scheibe P, Köhler B, Allgeier S, Guthoff RF, Stachs O. Local variability of parameters for characterization of the corneal subbasal nerve plexus. Curr Eye Res 2016;41(2):186–98. https://doi.org/10.3109/02713683.2015.1010686
[10] Allgeier S, Winter K, Bretthauer G, Guthoff RF, Peschel S, Reichert K-M, Stachs O, Köhler B. A novel approach to analyze the progression of measured corneal subbasal nerve fiber length in continuously expanding mosaic images. Curr Eye Res 2017;42(4):549–56. https://doi.org/10.1080/02713683.2016.1221977
[11] Martinez-Conde S, Macknik SL, Hubel DH. The role of fixational eye movements in visual perception. Nat Rev Neurosci 2004;5(3):229–40. https://doi.org/10.1038/nrn1348
[12] Baghaie A, Yu Z, D'Souza RM. Involuntary eye motion correction in retinal optical coherence tomography: hardware or software solution? Med Image Anal 2017;37:129–45. https://doi.org/10.1016/j.media.2017.02.002
[13] Bowers NR, Boehm AE, Roorda A. The effects of fixational tremor on the retinal image. J Vis 2019;19(11):8. https://doi.org/10.1167/19.11.8
[14] Zhivov A, Blum M, Guthoff R, Stachs O. Real-time mapping of the subepithelial nerve plexus by in vivo confocal laser scanning microscopy. Br J Ophthalmol 2010;94(9):1133–5. https://doi.org/10.1136/bjo.2009.175489
[15] Edwards K, Pritchard N, Gosschalk K, Sampson GP, Russell A, Malik RA, Efron N. Wide-field assessment of the human corneal subbasal nerve plexus in diabetic neuropathy using a novel mapping technique. Cornea 2012;31(9):1078–82. https://doi.org/10.1097/ICO.0b013e318245c012
[16] Turuwhenua JT, Patel DV, McGhee CNJ. Fully automated montaging of laser scanning in vivo confocal microscopy images of the human corneal subbasal nerve plexus. Invest Ophthalmol Vis Sci 2012;53(4):2235–42. https://doi.org/10.1167/iovs.11-8454
[17] Poletti E, Wigdahl J, Guimarães P, Ruggeri A. Automatic montaging of corneal subbasal nerve images for the composition of a wide-range mosaic. In: Proceedings of the 2014 36th annual international conference of the IEEE engineering in medicine and Biology society. Piscataway, NJ: IEEE; 2014. p. 5426–9. https://doi.org/10.1109/EMBC.2014.6944853
[18] Allgeier S, Bartschat A, Bohn S, Peschel S, Reichert K-M, Sperlich K, Walckling M, Hagenmeyer V, Mikut R, Stachs O, Köhler B. 3d confocal laser-scanning microscopy for large-area imaging of the corneal subbasal nerve plexus. Sci Rep 2018;8:7468. https://doi.org/10.1038/s41598-018-25915-6
[19] Allgeier S, Bartschat A, Bohn S, Guthoff RF, Hagenmeyer V, Kornelius L, Mikut R, Reichert K-M, Sperlich K, Stache N, Stachs O, Köhler B. Real-time large-area imaging of the corneal subbasal nerve plexus. Sci Rep 2022;12:2481. https://doi.org/10.1038/s41598-022-05983-5
[20] Bedggood P, Wu M, Zhang X, Rajan R, Wu CY, Karunaratne S, Metha AB, Mueller SN, Chinnery HR, Downie LE. Improved tracking of corneal immune cell dynamics using in vivo confocal microscopy. Biomed Opt Express 2024;15(11):6277–98. https://doi.org/10.1364/BOE.536553
[21] Li G, Li T, Li F, Zhang C. NerveStitcher: corneal confocal microscope images stitching with neural networks. Comput Biol Med 2022;151:106303. https://doi.org/10.1016/j.compbiomed.2022.106303
[22] Qiao Y, Li G, Li F, Zhang C. Nervestitcher2.0: evolution of stitching algorithm for corneal confocal microscope images with optical flow. In: Proceedings of the 2023 8th international conference on biomedical imaging, signal processing. New York, NY: ACM; 2023. p. 46–54. https://doi.org/10.1145/3634875.3634882
[23] Loewke KE, Camarillo DB, Piyawattanametha W, Mandella MJ, Contag CH, Thrun S, Salisbury JK. In vivo micro-image mosaicing. IEEE Trans Biomed Eng 2011;58(1):159–71. https://doi.org/10.1109/TBME.2010.2085082
[24] Chiang JCB, Khou V, Tavakoli A, Park SB, Goldstein D, Krishnan AV, Markoulli M. Reproducibility and reliability of subbasal corneal nerve parameters of the inferior whorl in the neurotoxic and healthy cornea. Cornea 2022;41(12):1487–94. https://doi.org/10.1097/ICO.0000000000002947
[25] Badian RA, Allgeier S, Scarpa F, Andréasson M, Bartschat A, Mikut R, Colonna A, Bellisario M, Utheim TP, Köhler B, Svenningsson P, Lagali N. Wide-field mosaics of the corneal subbasal nerve plexus in parkinson's disease using in vivo confocal microscopy. Sci Data 2021;8:306. https://doi.org/10.1038/s41597-021-01087-3
[26] Hao R, Liu Z, Chou Y, Huang C, Jing D, Wang H, Gao S, Li X. Analysis of globular cells in corneal nerve vortex. Front Med 2022;9:806689. https://doi.org/10.3389/fmed.2022.806689
[27] Lagali NS, Allgeier S, Guimarães P, Badian RA, Ruggeri A, Köhler B, Utheim TP, Peebo B, Peterson M, Dahlin LB, Rolandsson O. Reduced corneal nerve fiber density in type 2 diabetes by wide-area mosaic analysis. Invest Ophthalmol Vis Sci 2017;58(14):6318–27. https://doi.org/10.1167/iovs.17-22257
[28] Lagali NS, Allgeier S, Guimarães P, Badian RA, Ruggeri A, Köhler B, Utheim TP, Peebo B, Peterson M, Dahlin LB, Rolandsson O. Wide-field corneal subbasal nerve plexus mosaics in age-controlled healthy and type 2 diabetes populations. Sci Data 2018;5:180075. https://doi.org/10.1038/sdata.2018.75
[29] Badian RA, Utheim TP, Lagali N. Region of interest and directional analysis of subbasal nerves in wide-area corneal nerve plexus mosaics in type 2 diabetes mellitus. Sci Rep 2020;10:10802. https://doi.org/10.1038/s41598-020-67737-5
[30] Takhar JS, Joye AS, Lopez SE, Marneris AG, Tsui E, Seitzman GD, Keenan JD, Gonzales JA. Validation of a novel confocal microscopy imaging protocol with assessment of reproducibility and comparison of nerve metrics in dry eye disease compared with controls. Cornea 2021;40(5):603–12. https://doi.org/10.1097/ICO.0000000000002549
[31] Nortey J, Tsang A, Lopez S, Gebreegziabher E, Keenan JD, Lietman T, Gonzales JA. Central corneal subbasal nerve plexus abnormalities in sjögren disease: a pilot study. Cornea 2023;42(11):1432–8. https://doi.org/10.1097/ICO.0000000000003248
[32] Sandvik SA, Morisbakk TL, Lundanes E, Lid J, Lagali N, Sundling V. Methods for the evaluation of corneal nerve fibres in diabetes mellitus by in vivo confocal microscopy: a scoping review. BMJ Open 2025;15(9):e098294. https://doi.org/10.1136/bmjopen-2024-098294
[33] Bohn S, Stache N, Sperlich K, Allgeier S, Köhler B, Bartschat A, Do H-V, George C, Guthoff RF, Stachs A, Stachs O, Sterenczak KA. In vivo monitoring of corneal dendritic cells in the subbasal nerve plexus during trastuzumab and paclitaxel breast cancer therapy—a one-year follow-up. Diagnostics 2022;12(5):1180. https://doi.org/10.3390/diagnostics12051180
[34] Stache N, Sterenczak KA, Sperlich K, Marfurt CF, Allgeier S, Köhler B, Mikut R, Bartschat A, Reichert K-M, Guthoff RF, Stachs A, Stachs O, Bohn S. Assessment of dynamic corneal nerve changes using static landmarks by in vivo large-area confocal microscopy—a longitudinal proof-of-concept study. Quant Imaging Med Surg 2022;12(10):4734–46. https://doi.org/10.21037/qims-22-15
[35] Schindelin J, Arganda-Carreras I, Frise E, Kaynig V, Longair M, Pietzsch T, Preibisch S, Rueden C, Saalfeld S, Schmid B, Tinevez J-Y, White DJ, Hartenstein V, Eliceiri K, Tomancak P, Cardona A. Fiji: an open-source platform for biological-image analysis. Nat Methods 2012;9(7):676–82. https://doi.org/10.1038/nmeth.2019
[36] Allgeier S, Maier S, Mikut R, Peschel S, Reichert K-M, Stachs O, Köhler B. Mosaicking the subbasal nerve plexus by guided eye movements. Invest Ophthalmol Vis Sci 2014;55(9):6082–9. https://doi.org/10.1167/iovs.14-14698
[37] Toso L, Allgeier S, Eberle F, Maier S, Reichert K-M, Köhler B. Iterative algorithms to generate large scale mosaic images. In: Handels H, Deserno TM, Meinzer H-P, Tolxdorff T, editors. Bildverarbeitung für die medizin 2015, Informatik aktuell. Berlin, Heidelberg: Springer Vieweg; 2015. p. 203–8. https://doi.org/10.1007/978-3-662-46224-9_36
[38] Allgeier S, Zhivov A, Eberle F, Köhler B, Maier S, Bretthauer G, Guthoff RF, Stachs O. Image reconstruction of the subbasal nerve plexus with in vivo confocal microscopy. Invest Ophthalmol Vis Sci 2011;52(9):5022–8. https://doi.org/10.1167/iovs.10-6065
[39] Allgeier S, Köhler B, Eberle F, Maier S, Stachs O, Zhivov A, Bretthauer G. Elastische registrierung von in-vivo-CLSM-aufnahmen DER kornea. In: Handels H, Ehrhardt J, Deserno TM, Meinzer H-P, Tolxdorff T, editors. Bildverarbeitung für die medizin 2011, Informatik aktuell. Berlin, Heidelberg: Springer; 2011. p. 149–53. https://doi.org/10.1007/978-3-642-19335-4_32
[40] Bartschat A, Toso L, Stegmaier J, Kuijper A, Mikut R, Köhler B, Allgeier S. Automatic corneal tissue classification using bag-of-visual-words approaches. In: Heizmann M, Längle T, Puente León F, editors. Forum bildverarbeitung 2016. Karlsruhe: KIT Scientific Publishing; 2016. p. 245–56. https://doi.org/10.5445/KSP/1000059899
[41] Badian RA, Lagali N, Allgeier S, Scarpa F, Andréasson M, Bartschat A, Mikut R, Colona A, Bellisario M, Paaske Utheim T, Köhler B, Svenningsson P. Wide-field mosaic dataset of the corneal subbasal nerve plexus in parkinson's disease using in vivo confocal microscopy, 2021. https://doi.org/10.6084/m9.figshare.14481249
[42] Sterenczak KA, Sperlich K, Bohn S, Schaub F, Stachs O. Early detection of subclinical corneal abnormalities: biophotonic imaging reveals hyporeflective bleb-like structures in asymptomatic eyes. Am J Case Rep 2024;25:e944321. https://doi.org/10.12659/AJCR.944321
[43] Sterenczak KA, Stachs O, Marfurt C, Matuszewska-Iwanicka A, Stratmann B, Sperlich K, Guthoff RF, Hettlich H-J, Allgeier S, Stahnke T. Atypical cellular elements of unknown origin in the subbasal nerve plexus of a diabetic cornea diagnosed by large-area confocal laser scanning microscopy. Diagnostics 2021;11(2):154. https://doi.org/10.3390/diagnostics11020154
[44] Matuszewska-Iwanicka A, Stratmann B, Stachs O, Allgeier S, Bartschat A, Winter K, Guthoff R, Tschoepe D, Hettlich H-J. Mosaic VS. Single image analysis with confocal microscopy of the corneal nerve plexus for diagnosis of early diabetic peripheral neuropathy. Ophthalmol Ther 2022;11(6):2211–23. https://doi.org/10.1007/s40123-022-00574-z
[45] Badian RA, Lagali N. The inferocentral whorl region and its directional patterns in the corneal sub-basal nerve plexus: a review. Exp Eye Res 2024;244:109926. https://doi.org/10.1016/j.exer.2024.109926
[46] Wu M, Zhang X, Karunaratne S, Lee J-H, Lampugnani ER, Selva KJ, Chung AW, Mueller SN, Chinnery HR, Downie LE. Intravital imaging of the human cornea reveals the differential effects of season on innate and adaptive immune cell morphodynamics. Ophthalmology 2024;131(10):1185–95. https://doi.org/10.1016/j.ophtha.2024.04.020
[47] Sperlich K, Bohn S, Worsch F, Colorado LH, Allgeier S, Stachs O. In vivo corneal microscopy: from image to insight – where are we going? Z Med Phys 2025:S0939388925001199. https://doi.org/10.1016/j.zemedi.2025.10.001